Supplementary Material

Supplementary Methods:

MCF10AT invasion assays:

MCF10AT cells were cultured in DMEM/F12 medium (Invitrogen) supplemented with 5% horse serum, 20 ng/ml EGF, 0.5 mg/ml hydrocortisone, 100 ng/ml cholera toxin, 100 μg/ml insulin and 1% penicillin/streptomycin. For organoid generation, single MCF10AT cells were plated in Matrigel (Corning) and allowed to develop for 14 days. MCF10AT spheroids were then dissociated with Dispase and co-cultured with dissociated GBM cells in neural maintenance medium in GravityTRAP ULA Plates, as described for neural organoid co-cultures.

SH-SY5Y invasion assays:

SH-SY5Y cells were cultured in neural maintenance medium (Methods). To generate spheroids, cells were plated in a GravityTRAP ULA Plate (PerkinElmer) at a density of 5,000 cells per well and allowed to develop for 7 days. SH-SY5Y spheroids were then co-cultured with dissociated GBM cells in neural maintenance medium, as described for neural organoid co-cultures.

Immunohistochemistry:

Immunohistochemistry was performed using standard protocols with primary antibodies against KI67 (BD Bioscience #610969), OCT4 (Abcam ab19857), βIII-tubulin (BioLegend #801202), PAX6 (BioLegend #901301), GPC3 (Sigma HPA006316), CD81 (Invitrogen MA5-13548), DLK1 (Invitrogen MA5-15915), NOTCH1 (CST 4380), COL4A5 (LSBio LS-C353940), ITGAV (Abcam ab16821), β-actin (Abcam ab8226), Cx43 (Sigma C6219), GFP (Abcam 13970), and appropriate secondary antibodies (Cell Signaling Technology).

Image analysis:

Image pre-processing was performed in ImageJ as follows: To obtain a representation of the organoid, the SiR-actin signal was subjected to brightness adjustment and Gaussian blurring (sigma = 2), followed by scaling to 2912 μm^3/voxel by bicubic interpolation, and binarization using the Triangle method. To identify the voxels occupied by GBM cells, the GFP signal was subjected to brightness adjustment and Rolling-Ball background subtraction (radius = 64), followed by scaling to 2912 μm^3/voxel by bicubic interpolation, and binarization using Otsu's method.

Downstream image processing was performed in MATLAB as follows: Using binarized images, single cells in the Matrigel surrounding organoids were excluded by connected component analysis using the 'bwlabeln' function, and holes inside the organoid were filled with the 'imfill' function. The organoid surface was approximated by Delauney triangulation using the 'delaunayTriangulation', and normal distances from GBM-occupied voxels to the organoid surface were calculated with the 'point2trimesh' function. We performed hierarchical clustering of voxels based on Euclidean distances and calculated distance matrices to visualize dispersion of GBM cells within organoids.

Processes were tracked using the Simple Neurite Tracer in ImageJ. A total of 120 cells (n=10 cells each from n=3 organoids for each patient) were randomly selected, and all their processes tracked.

scRNA-seq:

Cell isolation and library preparation: Single-cell suspensions were stained with Hoechst and Propidium Iodide (ReadyProbe Cell Viability Imaging Kit, Invitrogen) for 10 min at room temperature and cell numbers and viability were checked with a Countess automated cell counter (Thermo Fisher). Samples were discarded if cell viability was below 85%. The TakaraBio iCELL8 system and the associated Rapid Development Protocol (in-chip RT-PCR amplification) were used for single cell isolation, reverse transcription and cDNA amplification[1]. Briefly, cell suspensions were distributed into a nanowell chip containing oligo-dT primers with a unique barcode for every well. Chips were imaged using an automated fluorescence microscope and frozen at -80°C until further use. Nanowells occupied by single cells were identified using the CellSelect software and manually curated in order to exclude non-detected doublets or dead cells. After thawing frozen chips, 50 nl of RT/Amp solution was dispensed into selected nanowells (Master mix: 56 µl 5 M Betaine, 24 µl 25 mM dNTP mix (TakaraBio), 3.2 µl 1 M $MgCl_2$ (Invitrogen), 8.8 µl 100 mM Dithiothreitol (TakaraBio), 61.9 µl 5x SMARTScribe™ first-strand buffer, 33.3 µl 2x SeqAmp™ PCR buffer, 4.0 µl 100 µM RT E5 Oligo, 8.8 µl 10 µM Amp primer (all TakaraBio), 1.6 µl 100% Triton X-100 (Acros), 28.8 µl SMARTScribe™ Reverse Transcriptase, 9.6 µl SeqAmp™ DNA Polymerase (TakaraBio)). After in-chip RT/Amp amplification (18 amplification cycles, in-chip RT/Amp Rapid Development protocol) inside a modified SmartChip Cycler (Bio-Rad), libraries were pooled, concentrated (DNA Clean and Concentrator−5 kit, Zymo Research) and purified using 0.6x Ampure XP beads. Concentration and quality of cDNA was assessed by a fluorometer (Qubit) and by electrophoresis (Agilent Bioanalyzer high sensitivity DNA chips). Next generation sequencing libraries were constructed using the Nextera XT kit (Illumina)

following the manufacturer´s instructions. Final libraries were sequenced with the NextSeq 500 system in high-output mode (paired-end, 21 x 70 for v1, 24 x 67 for v2 chip).

scRNA-seq data analysis:

Pre-processing, quality control and normalization: For pre-processing of single-cell RNA-seq data, an automated in-house workflow based on Roddy (https://github.com/TheRoddyWMS/Roddy) was used. Read quality was evaluated using FastQC. iCELL8 library barcodes from the first 21 bp reads were assigned to the associated nanowell with the Je demultiplexing suite[2]. Remaining primer sequences, Poly-A/T tails and low-quality ends (<25) were trimmed using Cutadapt. Furthermore, since NextSeq (Illumina) encodes undetected bases as incorrect 'Gs' with high quality, Cutadapt's '—nextseq-trim' option was used for improved quality trimming. Trimmed reads were mapped to the reference genome hs37d5 (derived from the 1000 genomes project) using the STAR aligner. Mapped BAM files were quantified using featureCounts with reference annotation gencode v19.
RNA-seq libraries that contained less than 150 detected genes or more than 15% mitochondrial reads were filtered out. Adapting a previously published approach[3], aggregate expression for each gene across all cells was calculated as $E_a = \log(\text{mean}[E_{j,1\ldots n}] + 1)$, where E_j is the counts-per-million expression value of the gene in cell j. 8,533 genes with $E_a > 2$ were retained for analysis.

Comparison of tumor cells from individual and co-cultured samples: Filtered and normalized data of all patients was combined to identify NPCs and tumor cells in each sample. Using the Seurat package as implemented in R[4], principal component analysis (PCA) was performed prior to clustering, and the 'FindClusters' function (with resolution = 0.4) was run on the first 9 principal components only. Results were visualized by tSNE[5]. Clusters containing cells from the NPC-only sample were identified as 'brain', whereas clusters containing only GBM cells were identified as 'tumor'. After manual splitting of one of the resulting clusters, we obtained 10 clusters representing brain cells (3 clusters), tumor cells from co-cultured samples, or tumor cells from unmixed samples. Differential expression between mixed and unmixed tumor cells was evaluated using the 'FindMarkers' function in Seurat. Gene set enrichment analysis[6] was performed by computing overlaps between identified gene signatures and Gene Ontology (GO_C5) gene sets derived from the Molecular Signature Database (MSigDB, https://software.broadinstitute.org/gsea/msigdb). Cell state signature genes for OPC, NPC, AC, MES, as well as G1/S and G2/M cell cycle phases were downloaded from a recent study[28]. Following their approach, cell state scores and cell cycle scores were computed using the AddModuleScore function in Seurat. GBM cells

were classified as OPC, NPC, AC or MES based on the highest cell state score. Cell cycle scores were calculated based on the combined list of G1/S and G2/M genes.

Analysis of ligand-receptor interactions: Potential receptor–ligand pairings were analyzed using 2,557 previously published receptor–ligand pairs consisting of 1,398 unique genes[7], of which 317 were expressed in our data. Adapting a previously published approach[8], we constructed a cell-cell interaction matrix by summing for each pair of cells from the same sample the number of ligand-receptor pairs potentially connecting the pair, with one cell type expressing the receptor and the other the ligand (normalized expression cutoff >0.5). To identify ligand-receptor interactions with likely significance for the invasion process, we then considered each ligand-receptor pair in turn, and calculated the number of cell pairs connected by this ligand-receptor interaction for each possible cell type combination (tumor–tumor, brain–brain, tumor–brain), for each sample. The resulting interaction matrix was normalized to the maximum possible number of cell-cell interactions. To identify ligand-receptor pairs with coherent differential expression across patients, we considered only those ligand-receptor pairs with mean normalized expression greater than 0.5 times the mean across all pairs for all tumor-only samples, all pairings from mixed samples where tumor cells express the ligand, all interactions from mixed samples where tumor cells express the receptor, or the NPC-only sample. These interactions were clustered based on complete linkage of Euclidean distances and visualized using the heatmap.2 package in R. For Gene Ontology (GO) analysis, we considered those ligand-receptor pairs with mean normalized expression greater than 0.5 times the mean across all pairs for one cell type interaction (GBM→NPC, NPC→GBM, GBM→GBM, NPC→NPC), and less than 0.5 times the mean for the other three. No putative GBM→GBM interactions fulfilled these criteria.

Supplementary Figures 1-7:

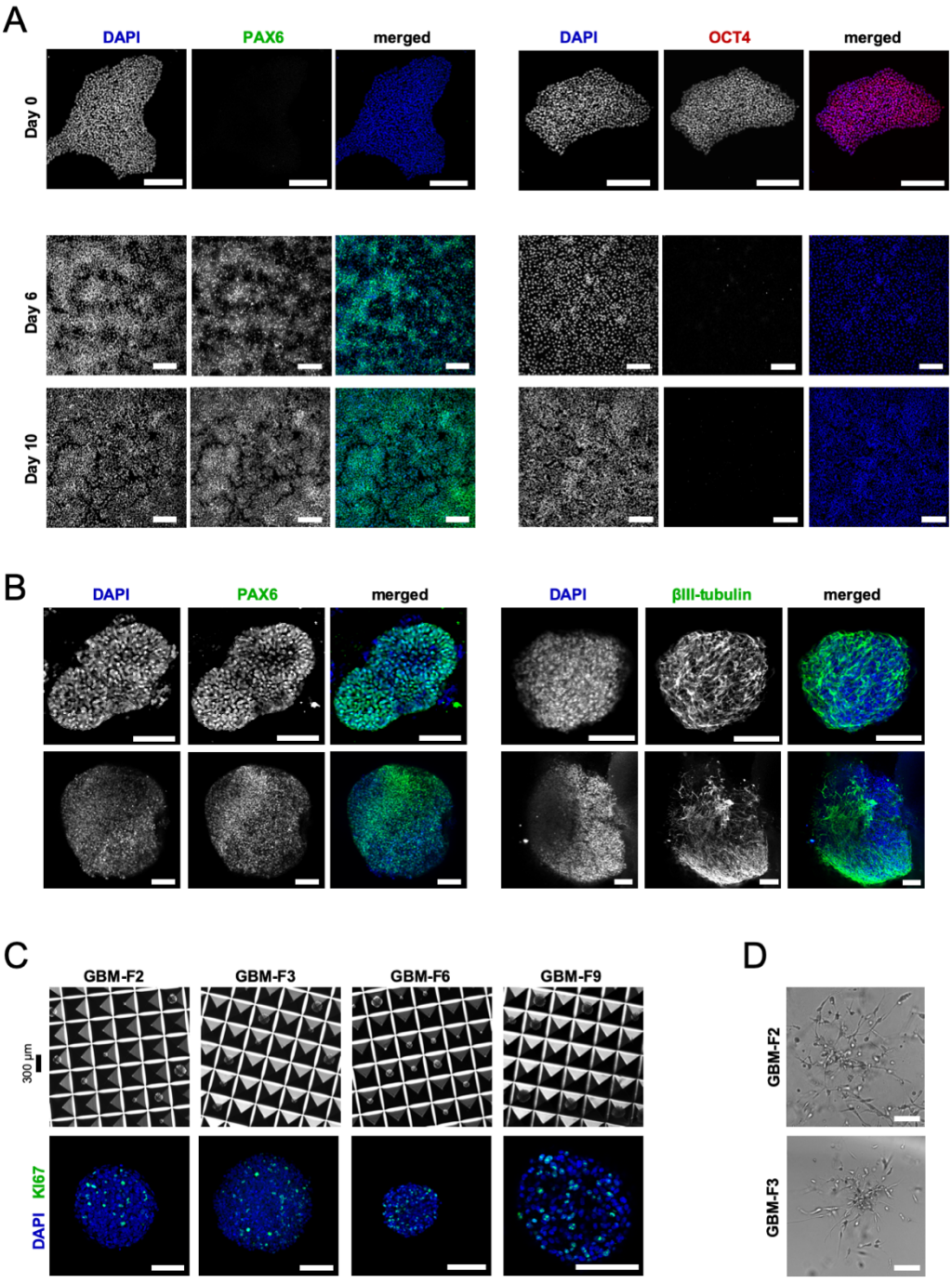

Supplementary Figure 1 | Characterization of cerebral organoid formation and patient-derived GBM cells. A) Neural induction of iPS cells in 2D resulted in downregulation of the pluripotency marker gene OCT4 and concurrent upregulation of the neural stem cell marker gene PAX6 within 6 days. Scale bars, 200 µm. **B)** Neural induction of iPS cells in 3D results in strong expression of PAX6 within 6 days (left). After 24 days of culture, organoids express the neuronal marker βIII-tubulin (right). Note that, unlike in the rest of the paper,

these organoids were grown from iPSC spheroids of varying sizes. Scale bars, 100 µm. **C)** Top: Single-cell suspensions from all four GBM cell lines were placed into microcavity (AggreWell™) plates at low density, to obtain 0 or 1 cell in most cavities, and cultured for 34 days. GBM cells formed spheroids of heterogeneous sizes, demonstrating that they retain proliferative potential *in vitro*. Bottom: GBM spheroids grown from single cells were subjected to immunohistochemistry for further characterization. GBM cells showed heterogeneous expression of the cell cycle marker KI67, confirming that at least some cells retain proliferative capacity. Scale bars, 100 µm. **D)** GBM cells plated as spheroids invade into Matrigel. Images were acquired 48 hours after plating. Scale bars, 100 µm.

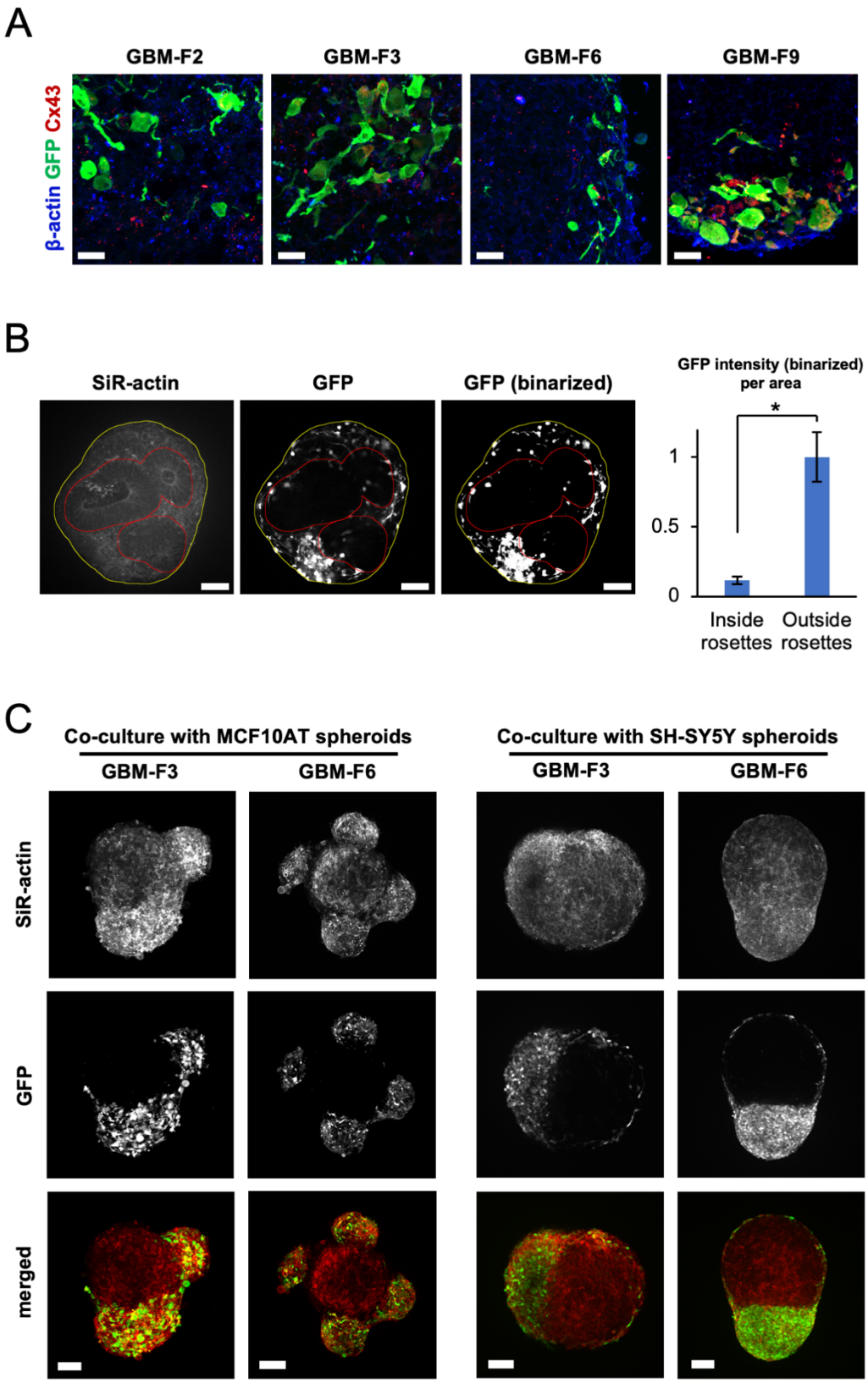

Supplementary Figure 2 | GBM invasion behaviour. **A)** GBM cells invaded into iPSC-derived cerebral organoids within 3 days. Expression of connexin-43 (Cx43) indicates gap junction formation. Scale bars, 20 µm. **B)** GBM cell invasion, as measured by binarized

GFP intensity per area, was quantified inside and outside of rosette structures (red and yellow lines, respectively) in image slices from 3 organoids for each of the 4 patient cell lines (scale bars, 100 μm). Bars represent mean values across n=12 samples, normalized to the mean outside of rosettes, and error bars represent standard errors in the mean (* $p < 0.001$, two-sided Student's t-test). **C)** GBM cells co-cultured with MCF10AT breast epithelial cell spheroids (left) or SH-SY5Y neuroblastoma spheroids (right) for 3 days showed no invasion (MCF10AT: F3, n=23; F6, n=18; SH-SY5Y: F3, n=17; F6, n=22). Representative images of co-cultures are shown for each patient-derived GBM cell line. Scale bars, 100 μm.

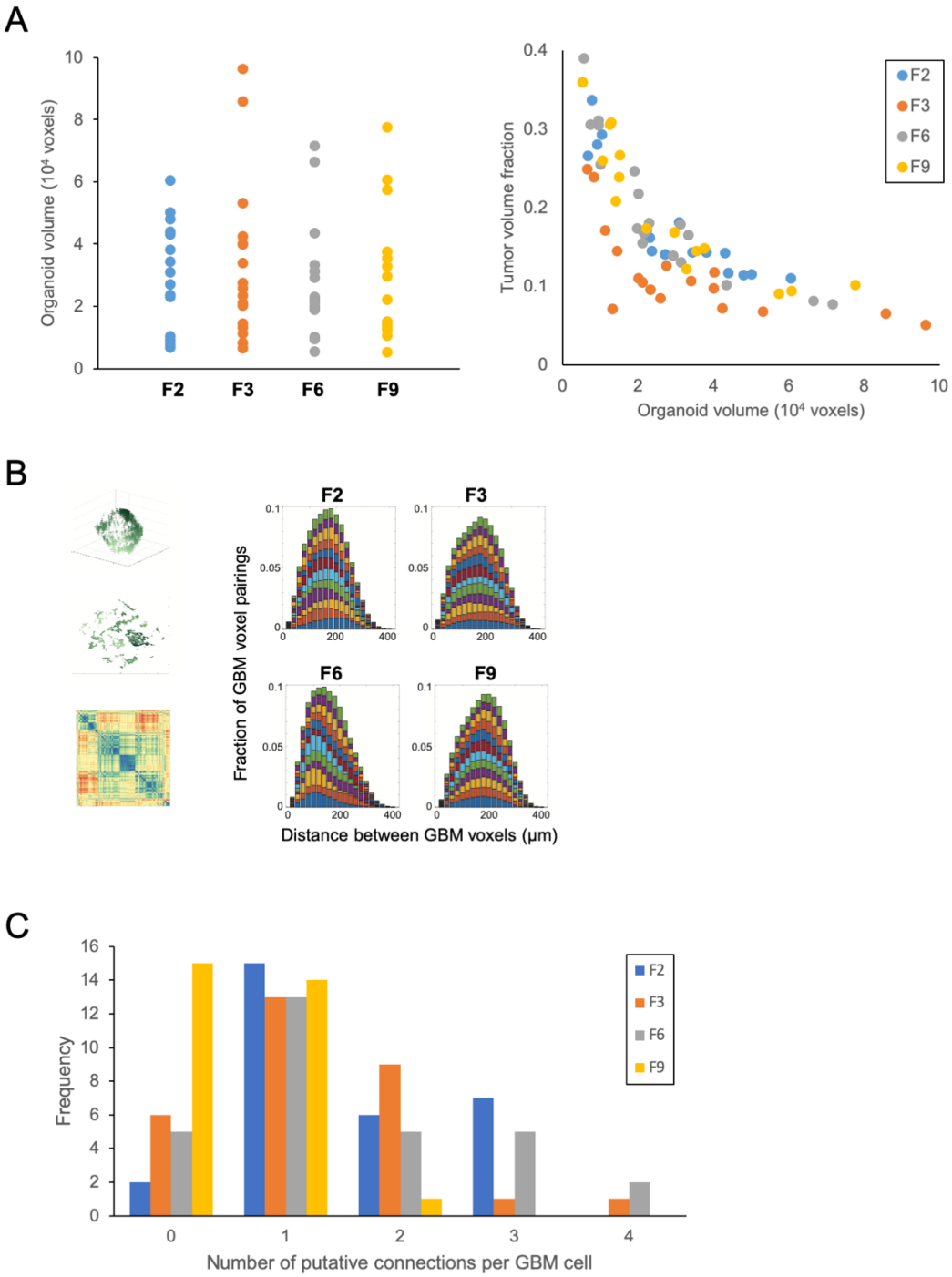

Supplementary Figure 3 | Quantification of GBM invasion into cerebral organoids. **A)** Organoids of similar sizes were selected for all four patient-derived GBM cell lines for experiments and quantification (left). A similar fraction of organoid volume was invaded by GBM cells from all four patient-derived cell lines (right). **B)** The distribution of distances between tumor voxels within organoids was similar for all four patient-derived cell lines. For visualization, a representative 3D rendering of GBM voxels is depicted (top left) along with a tSNE projection (below) and the corresponding distance matrix (bottom left). The distribution of distances between tumor voxels is shown for 12 representative organoids for each patient-derived cell line, with 500-900 µm diameter (right). **C)** Putative intratumoral connections, i.e. microtubes ending at other tumor cells, ranged in number from 0 to 4 per GBM cell.

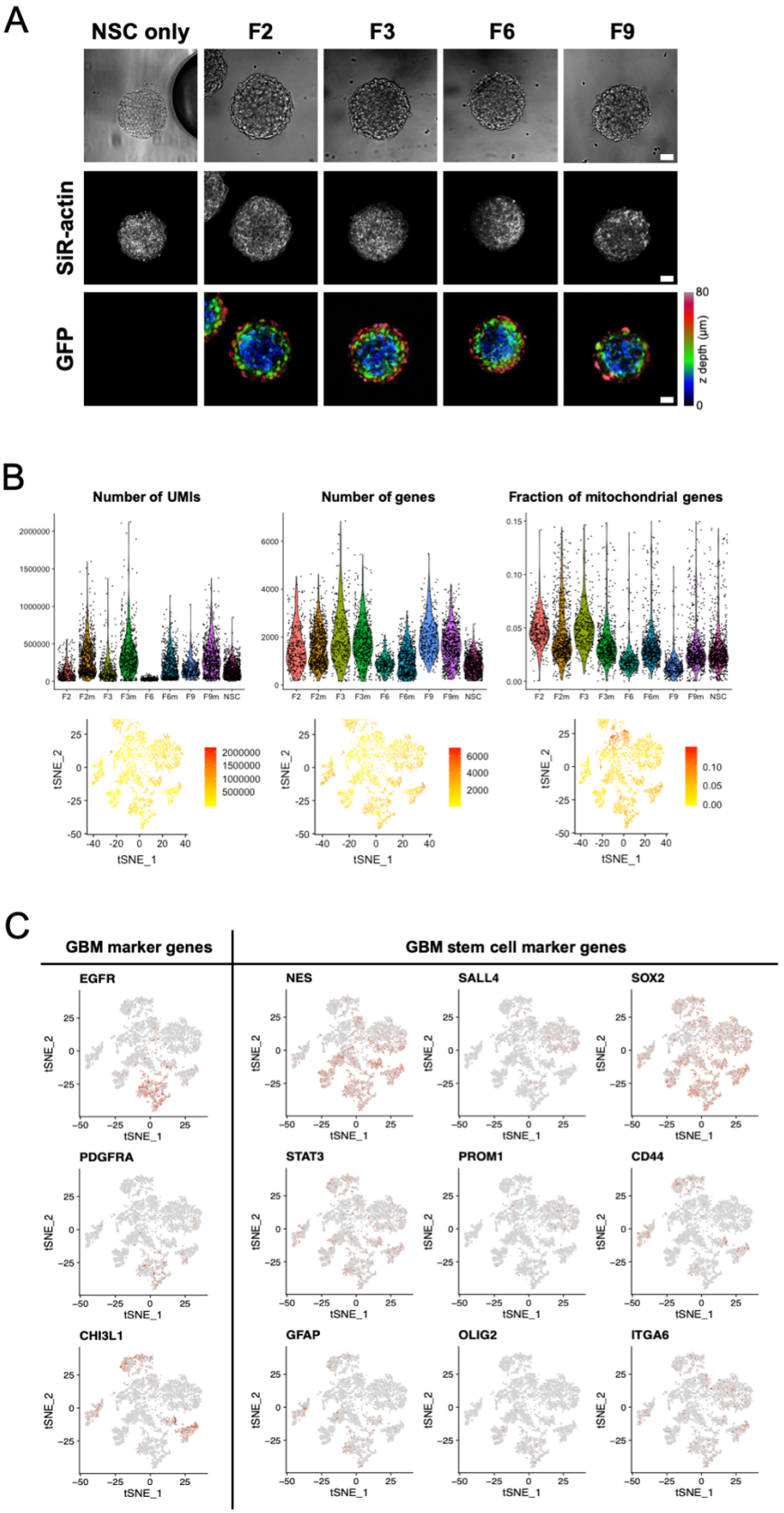

Supplementary Figure 4 | scRNA-seq analysis of GBM co-cultured with organoid cells. **A)** Tumor cells from all patient cell lines mix efficiently with organoid cells. Scale bars, 50 µm. **B)** Top row shows the number of UMIs, the number of genes, and the percentage of

mitochondrial genes in each sample. Bottom row shows the same variables visualized on a tSNE map of all cells (identical to the tSNE representation shown in Fig. 3D). **C)** Expression of putative GBM marker genes (left) and putative GBM stem cell marker genes (right) visualized on a tSNE map (identical to the tSNE representation shown in Fig. 3D; grey, low expression; red, high expression).

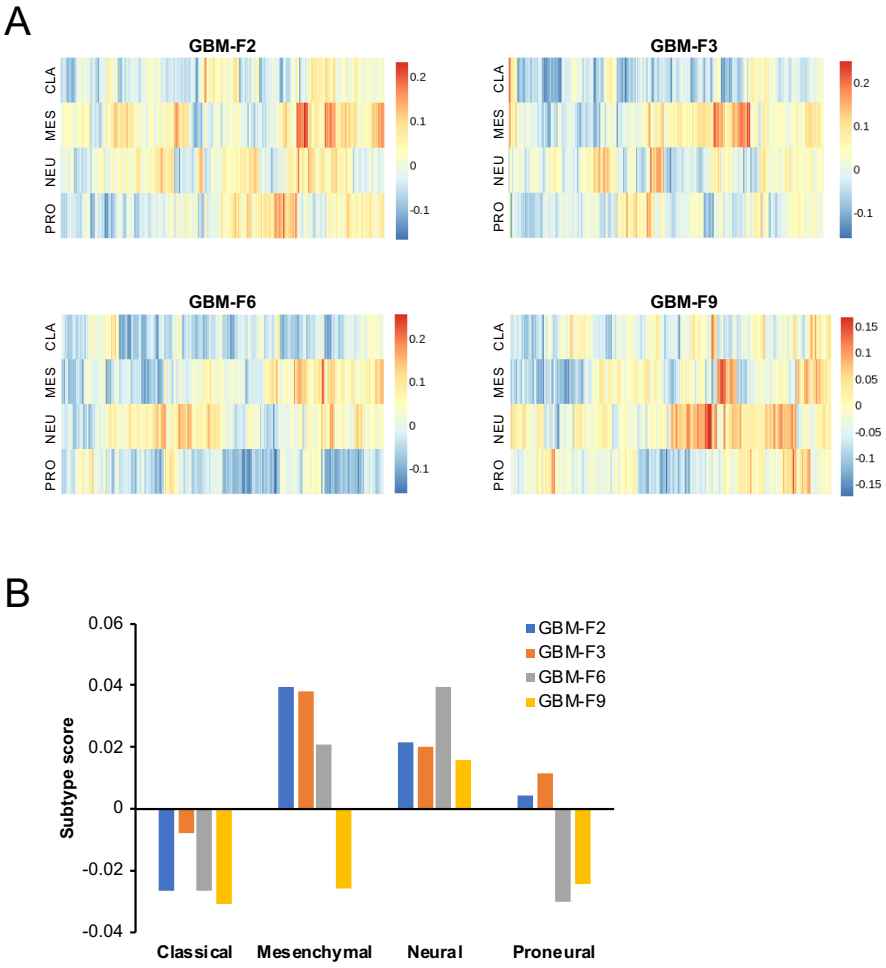

Supplementary Figure 5 | GBM subtype analysis of patient-derived cell lines. **A)** Subtype scores for the classical (CLA), mesenchymal (MES), neural (NEU) and proneural (PRO) GBM subtypes were computed for each cell based on the expression of 210 subtype signature genes[10], relative to the aggregated expression of control gene sets expressed at similar levels (Methods) . **B)** Average subtype scores for each patient-derived GBM cell line.

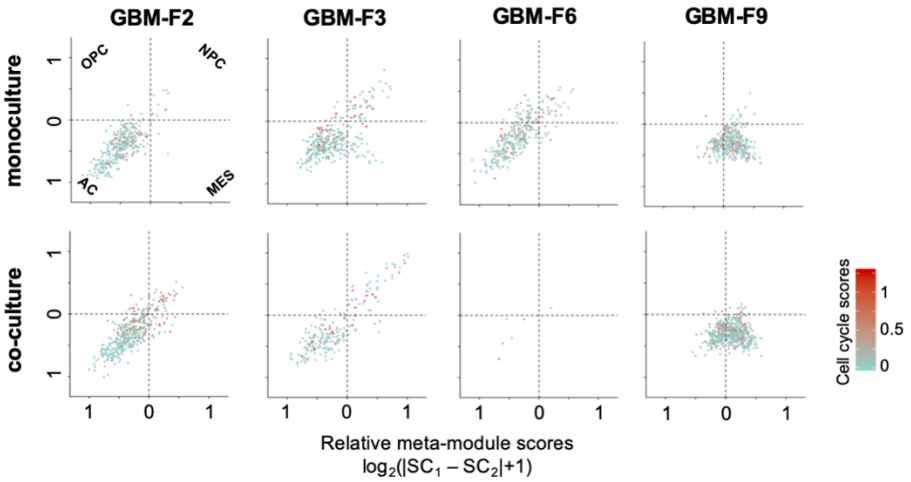

Supplementary Figure 6 | Changes in GBM cell states upon co-culture. Two-dimensional representation of cellular states, as defined in a previous study[28]. Each dot represents one cell, placed in the quadrant most representative of its transcriptional profile (OPC = oligodendrocytic precursor cell-like; NPC = neural progenitor cell-like; AC = astrocyte-like; MES = mesenchymal-like). Coordinates represent relative cell state scores and colors indicate cell cycle scores (Methods).

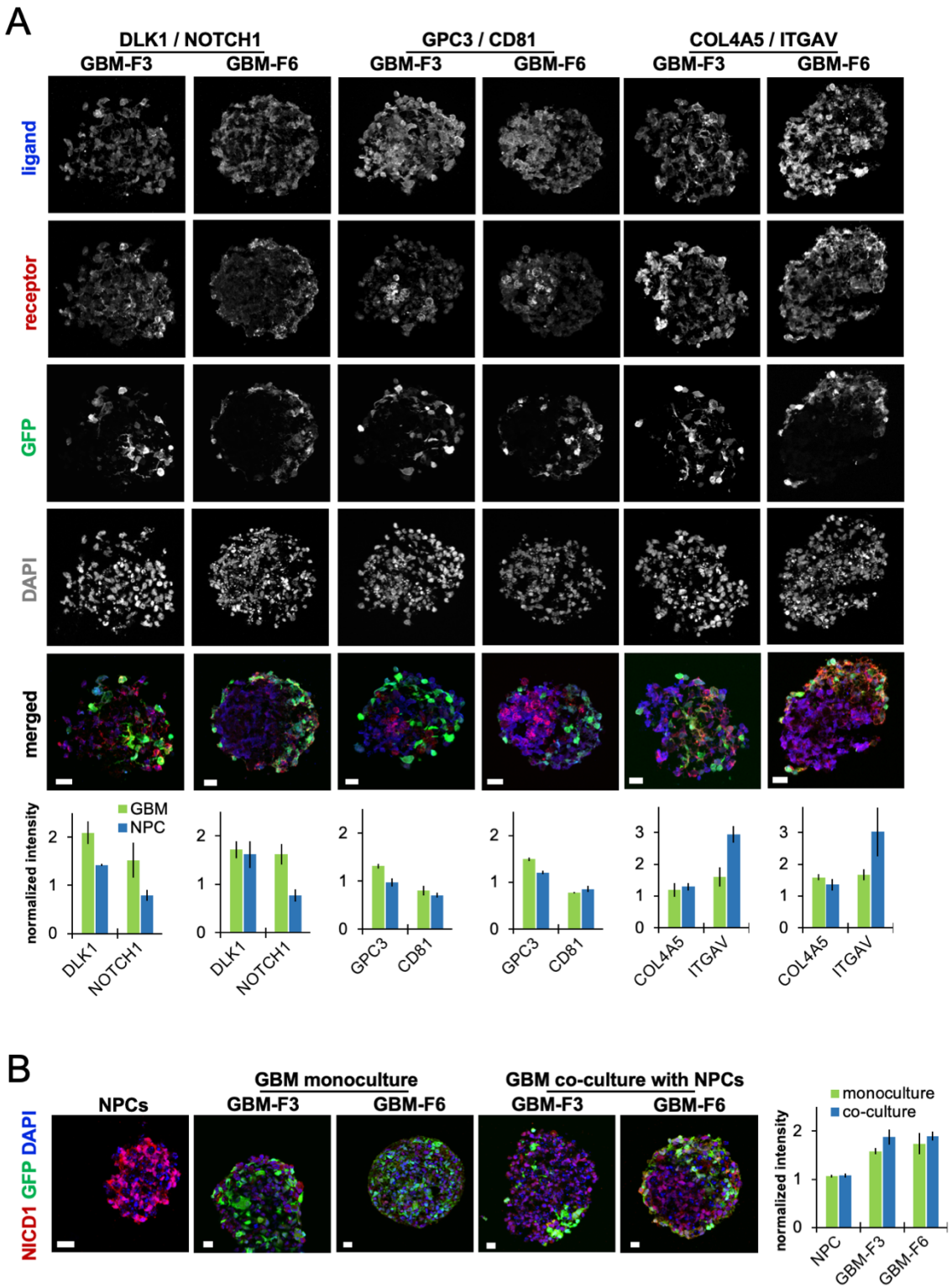

Supplementary Figure 7 | Changes in GBM ligand-receptor pair expression upon co-culture. **A)** Immunohistochemistry images show expression of ligand-receptor pairs in cryosections of co-culture spheroids comprising NPCs and GBM cells from patients F3 or F6. The bottom images merge ligand, receptor and GFP channels. Scale bars, 20 μm. Bar plots indicate the average intensity of ligands and receptors, normalized to DAPI intensity, across five images from each patient, in GBM cells (defined by GFP expression) and NPCs. Error

bars indicate SEM. **B)** Immunohistochemistry images show expression of NICD1 (the cleaved intracellular domain of NOTCH1), indicating NOTCH1 activation, in cryosections of monoculture and co-culture spheroids comprising NPCs and GBM cells from patients F3 or F6. Scale bars, 20 μm. Bar plots indicate the average NICD1 intensity, normalized to DAPI intensity, across two to five images per condition, in GBM cells (defined by GFP expression) and NPCs. Error bars indicate SEM.

Supplementary Table 1:

Cell line	**Classification**	**Primary/ Recurrence**	**Sex**	**Age**	**Localization**	**Treatment**	**IDH^{-}** (1)	**ATRX^{+}** (2)	**MGMT promoter methylation**
GBM-F2	Glioblastoma, WHO grade IV	Primary tumor	M	65	left occipital	none	✓	✓	✓
GBM-F3	Glioblastoma, WHO grade IV	Recurrence (after resection and re-resection)	M	52	right occipital	Radio-chemotherapy and surgery	✓	✓	unknown
GBM-F6	Glioblastoma, WHO grade IV	Primary tumor	M	68	right temporo-parietal	none	✓	✓	✓
GBM-F9	Glioblastoma, WHO grade IV (giant cell component)	Primary tumor	F	71	right temporal	none	✓	✓	✓

(1) No expression of IDH1_R132H detected.

(2) Expression of ATRX detected.

Supplementary Table 2:

Genes coherently upregulated in GBM cell lines upon co-culture with organoid cells:

GPC3	ANKRD36C
CRABP1	MORF4L2
CRABP2	EIF2S3
PLP1	POLA1
PLCH1	PUM1
ARGLU1	NKTR
TMOD3	VPS13B
RPS6	DDX3X

EIF4A2	COPA
RPL9	LARS
IGF2BP1	VPS41
ARRDC3	PAX6
SCG5	HSP90AB1
PSAP	PRUNE2
TMSB15A	GNPDA1
SPAG9	HSP90AA1
DLK1	CRYAB
LIX1	BLOC1S5
ANKRD36	GJA1
SUGP2	COL4A5
PRTG	LAMP2
HSPA8	KDM4A
POLR2B	

Supplementary Videos 1-4:

Representative example z-scans of cleared organoids after GBM invasion from the four patient cell lines (1: F2, 2: F3, 3: F6, 4: F9).

Supplementary References

1. Goldstein LD, Chen YJJ, Dunne J, et al. Massively parallel nanowell-based single-cell gene expression profiling. *BMC Genomics*. 2017;18(1):1-10.
2. Girardot C, Scholtalbers J, Sauer S, Su SY, Furlong EEM. Je, a versatile suite to handle multiplexed NGS libraries with unique molecular identifiers. *BMC Bioinformatics*. 2016;17(1):4-9.
3. Puram S V., Tirosh I, Parikh AS, et al. Single-Cell Transcriptomic Analysis of Primary and Metastatic Tumor Ecosystems in Head and Neck Cancer. *Cell*. 2017;171(7):1611-1624.
4. Macosko EZ, Basu A, Trombetta JJ, et al. Highly Parallel Genome-wide Expression Profiling of Individual Cells Using Nanoliter Droplets. *Cell*. 2015;161(5):1202-1214.
5. van der Maaten L, Hinton G. Visualizing Data using t-SNE. *J Mach Learn Res*. 2008;9:2579-2605.

6. Subramanian A, Tamayo P, Mootha VK, et al. Gene set enrichment analysis: A knowledge-based approach for interpreting genome-wide expression profiles. *Proc Natl Acad Sci*. 2005;102(43):15545-15550.

7. Ramilowski JA, Goldberg T, Harshbarger J, et al. A draft network of ligand–receptor-mediated multicellular signalling in human. *Nat Commun*. 2015;6:7866.

8. Camp JG, Sekine K, Gerber T, et al. Multilineage communication regulates human liver bud development from pluripotency. *Nature*. 2017;546(7659):533-538.

9. Mooney KL, Choy W, Sidhu S, et al. The role of CD44 in glioblastoma multiforme. *J Clin Neurosci*. 2016;34:1-5.

10. Verhaak RGW, Hoadley KA, Purdom E, et al. Integrated Genomic Analysis Identifies Clinically Relevant Subtypes of Glioblastoma Characterized by Abnormalities in PDGFRA, IDH1, EGFR, and NF1. *Cancer Cell*. 2010;17(1):98-110.